

Optimizing phosphorus-doped polysilicon in TOPCon structures using silicon oxide layers to improve silicon solar cell performance

Wangchao Wan, Jindou Shi, Yixi Liang, Chen Zhang, Zheyuan Da, Junnan Wang, Qing Yao, Youlong Xu, Minqiang Wang*

Electronic Materials Research Laboratory, Key Laboratory of the Ministry of Education International Center for Dielectric Research&Shannxi Engineering Research Center of Advanced Energy Materials and Devices, Xi'an Jiaotong University, 710049, Xi'an, China



ARTICLE INFO

Keywords:
Passivating contact
Double poly-Si/SiO_x
PECVD
N-situ phosphorus doping

ABSTRACT

Tunnel Oxide Passivated Contact (TOPCon) technology is one of the most influential and industrially viable solar cell technologies available today. Improving the quality of passivation contact has become a central focus of current research. Although the conventional monolayer polycrystalline silicon method is highly effective in TOPCon solar cells, it is limited by doping inhomogeneity, which impairs the passivation and electrical properties, and the cell's photovoltaic conversion efficiency remains suboptimal. To address this issue, this study investigates the deposition of two layers of silicon oxide and two layers of in-situ doped phosphorus amorphous silicon, termed double poly-Si/SiO_x structures, on n-type silicon wafers using plasma-enhanced chemical vapor deposition (PECVD). The effectiveness of the structure was confirmed through various characterization techniques such as scanning electron microscopy (SEM), X-ray diffraction (XRD), and X-ray photoelectron spectroscopy (XPS). Key findings indicate that the double-polysilicon structure significantly enhances the uniformity of phosphorus doping, improving the carrier lifetime of the cell and reducing the contact resistance. As a result, the average efficiency in the final production stage has a conversion efficiency gain of 0.23 % over the baseline group. This study underscores the potential of this PECVD methodology to advance the fabrication of high-efficiency solar cells by providing significant improvements in passivation, doping uniformity, and overall cell performance.

1. Introduction

Tunnel Oxide Passivated Contact (TOPCon) structures have become standard components for industrial applications in the solar cell industry [1,2]. Its special backside passivated contact structure effectively reduces carrier losses on the backside of the cell [3,4]. Typically, TOPCon's superb surface and chemical passivation is attributed to a heavily doped polysilicon layer and an ultrathin tunneled SiO_x layer (1.4–1.8 nm), which results in TOPCon contacts can achieve a very low surface recombination current density (J_0) of less than 1 fA/cm² [5]. In addition, calculations carried out by the German Solar Energy Research Institute in Hamelin show that the theoretical efficiency limit of TOPCon cells is 28.7 % [6]. This shows that TOPCon solar cells have great potential for increasing the efficiency of photovoltaic conversion.

Considering the cost and performance, the predominant preparation methods in the industry today are LPCVD and PECVD [7,8]. As the technology continues to evolve, PECVD methods have shown superior

performance [9–11]. Evidence for this includes higher film deposition rates, minimized winding, and lower equipment consumable costs [12, 13]. Therefore, the preparation of ultrathin oxide layers and heavily doped polysilicon films by PECVD in situ doping has received more attention. In the review report by Basnet et al. [5], a multilayer oxidized attempted passivation structure was mentioned, which resulted in a more uniform distribution of boron in the boron-doped polysilicon layer and reduced boron internal diffusion through the introduction of a silicon oxide layer. The passivation performance was significantly reduced from $J_0 = 23$ fA/cm² to $J_0 = 11$ fA/cm². Pham et al. [14,15] proposed a quantum well consisting of a stack of SiO_x/nanocrystalline silicon (nc-Si)/SiO_x layers between n a polycrystalline silicon (poly-Si) layer. Using a nanocrystalline silicon (nc-Si) layer as a buffer layer, the quantum well with a double silicon oxide layer plays an important role as a double potential barrier during the high-temperature annealing process, thus suppressing doping in-expansion into crystalline silicon to significantly improve the passivation quality, yielding an $iVoc$ as high as

* Corresponding author.

E-mail address: mqwang@xjtu.edu.cn (M. Wang).

742 mV and a J_0 as low as 1.1 fA/cm². The relative solar cell conversion efficiency is nearly 1 % higher than the baseline. S.MA et al. [16] solved the problem of polycrystalline silicon bursting film blistering by using PECVD in-situ phosphorus doped double polysilicon films, but did not optimize the uniformity of the phosphorus doping concentration of the underlying polysilicon, which is a worthwhile problem to be investigated. Glatthaar et al. [17] used the structure of multilayer polysilicon/silicon oxide to reveal that the silicon oxide layer can effectively prevent the burn-through phenomenon of silver paste, and made an in-depth study on the metallization of multilayer polysilicon/silicon oxide, but did not reflect the effect on the solar cell end of the spectrum. These issues are worthy of further study and discussion.

Through the above problems, this study proposes a new passivation structure (Fig. 2(b)): SiO_x/Poly (lightly doped)/SiO_x/Poly (heavily doped) as a double polysilicon/silicon oxide film by utilizing in situ phosphorus doped deposition by PECVD technology. Silicon oxide retards the diffusion of phosphorus into silicon wafers [18]. According to this theory, a second layer of silicon oxide helps to fabricate underlying polysilicon films with tunable and more uniform in situ doping concentrations [19]. In addition, the excellent passivation performance parameters with an average $iVoc = 744$ mV and $J_0 = 5.4$ fA/cm² were obtained using passivation test wafers with double poly-Si/SiO_x structure. Finally, an industrial-scale TOPCon solar cell was fabricated using a 183 × 183 mm² wafer with a double poly-Si/SiO_x structure, achieving an average conversion efficiency increase of 0.23 % in the production phase compared to the baseline groups. The results of this study highlight the great potential of double polysilicon/silicon oxide structures developed by PECVD in-situ deposition and their suitability for the production of high-efficiency TOPCon solar cells in industrial applications.

2. Experimental methods

To evaluate the performance of the underlying phosphorus-doped polysilicon in a double multilayer polysilicon/silicon oxide structure, backside passivation layers were prepared on n-type wafers with dimensions of 183 × 183 mm² (M10), a thickness of 130 ± 10 μm, and a resistivity of 0.7–1.2 Ω cm. The wafers were first polished with an alkaline solution. Subsequently, the wafers were prepared using the industrial TOPCon method, which confirms that the experimental

methodology is consistent with practical applications in industrial production lines. Therefore, this work is of greater significance.

2.1. Preparation of double poly silicon/silicon oxide structures

Fig. 1 illustrates the fabrication process used to create the passivation contact structure on the backside of a TOPCon solar cell. Prior to the deposition of the passivation layer, the wafers are alkali polished to obtain a polished wafer interface on an industrial production line. Subsequently, the preparation of the silicon oxide layer and the in-situ P-doped amorphous silicon layer on the backside of the wafer was carried out by means of PECVD (W25851, HORIS). The deposition temperature was 470 °C and various precursor gases were used, including N₂O, SiH₄, PH₃, and H₂. The thickness of the underlying silicon oxide was the same for both the baseline and experimental groups, with a thickness of 1.5 nm and a deposition time of 180 s. For the sample set of double polysilicon/silicon oxide (subsequently referred to as the experimental group), the thickness of the second layer of silicon oxide was also standardized with a deposition time of 120 s. For comparison purposes, we chose the TOPCon structure standardized on the production line as the baseline group, as shown in **Fig. 1**.

In the baseline group, the samples were structured with single poly-Si structures (SiO_x/poly-Si), where the flow of PH₃ was set to 1500 sccm. For the experimental group, all samples were structured with a double polysilicon/silicon oxide layer defined as SiO_x/poly-Si (lightly doped)/SiO_x/poly-Si (heavily doped). And three sets of samples, S1, S2 and S3, were prepared to obtain different doping concentrations of the underlying amorphous silicon. Since the phosphorus doping concentration of the bottom polysilicon layer is highly dependent on the phosphorus doping concentration of the top polysilicon layer, the PH₃ flow rate of the first polysilicon layer for all experimental samples was set to 300 sccm. For the second polysilicon layer of the experimental group, the PH₃ flow rate was set to 1000 sccm, 2000 sccm, and 3000 sccm for the sample groups S1, S2, and S3, respectively, in order to attain the desired level of doping with phosphorus. The polysilicon thickness was 120 nm for the baseline group and 65 nm for the first layer and 55 nm for the second layer in the experimental group. Finally, all samples were annealed in a nitrogen (N₂) environment (D12661, HORIS) at 900 °C for 60 min. This process converts amorphous silicon into polycrystalline silicon while activating the dopant.

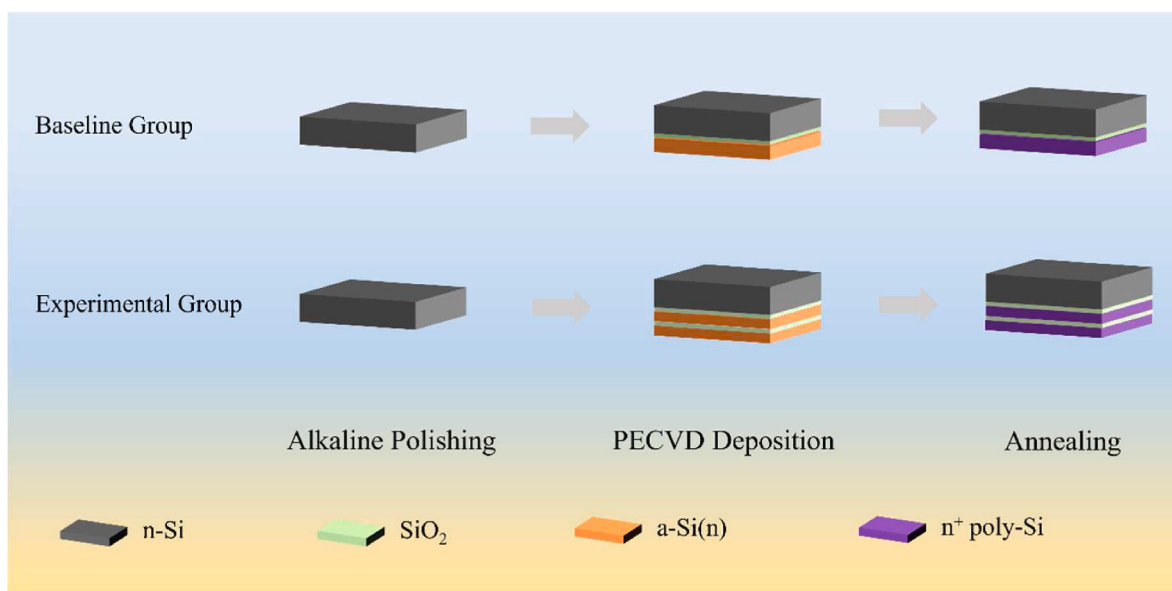


Fig. 1. illustrates the fabrication process for two contact types: baseline Group (n⁺ Poly/SiO_x/n-Si) and experimental Group (n⁺ Poly/SiO_x/n⁺ Poly/SiO_x/n-Si). The process begins with alkaline polishing, and Silicon oxide growth and deposition of P-doped amorphous silicon were then performed by PECVD. Finally, annealing to form the n⁺ polysilicon layer.

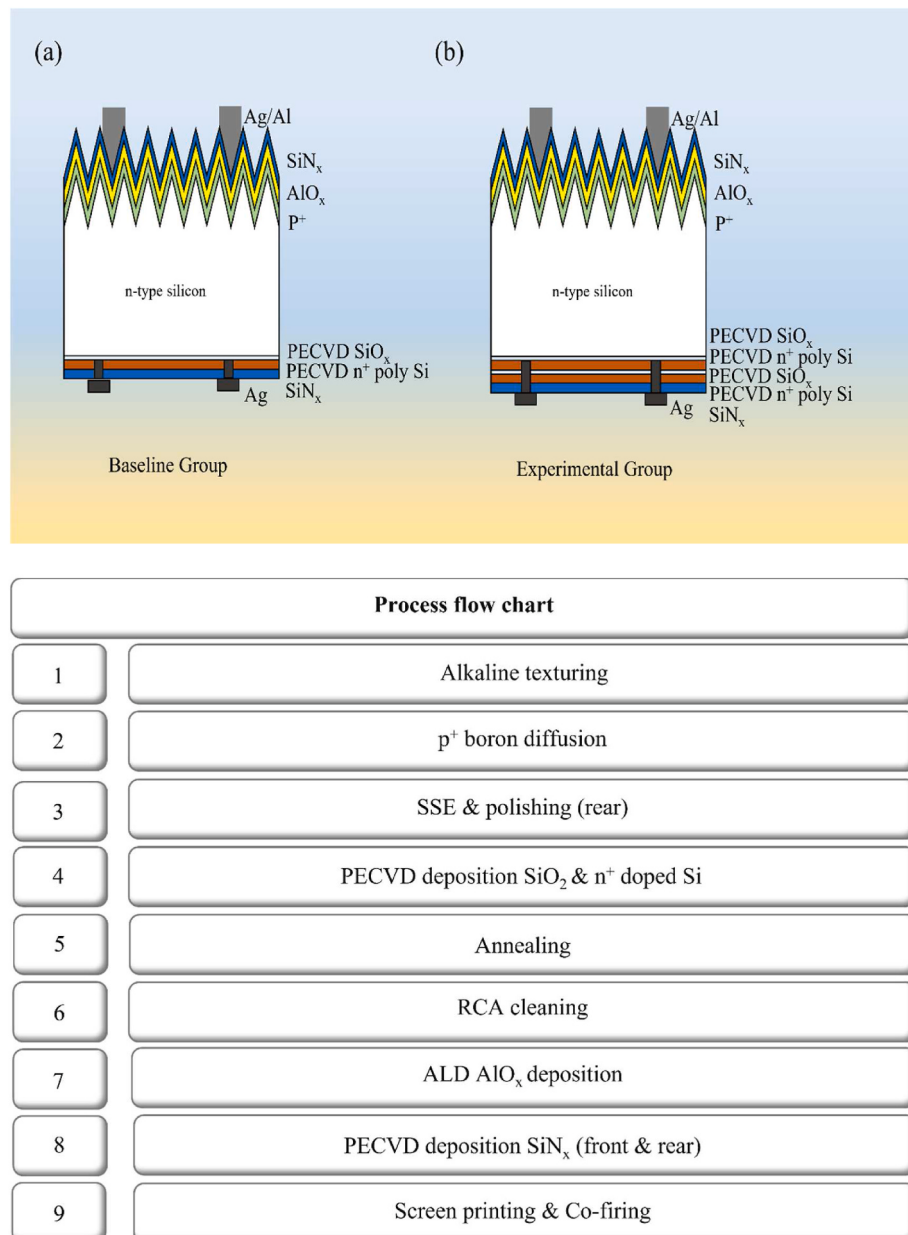


Fig. 2. (a) and (b) Schematic diagrams of the TOPCon cell structure for the baseline groups and experimental groups, respectively. The process flow chart is a diagram of the cells produced on an industrial production line.

2.2. Solar cell fabrication

In order to study the properties of poly-Si/SiO_x structures on devices, Fig. 2(a) shows the structural diagram of a TOPCon cell, and Fig. 2(b) shows the structural diagram of a TOPCon cell with a passivated structure of a double polysilicon/silicon oxide layer. The manufacturing process on the production line is as follows, as illustrated in Fig. 2, which depicts the process flow chart: (1) First, the n-type wafer is surface textured in potassium hydroxide (KOH) to form pyramids with a size of about 1.5 μm (2) After texturing, the p⁺ layer is formed on the front side of the wafer by boron diffusion equipment. (3) Subsequently, embedded single-side etching (SSE) removes the surrounding p⁺ doping before polishing the back surface with an alkaline solution. (4) Deposition of silicon oxide and doped amorphous silicon on the backside of the wafer using the PECVD method. (5) Then, the wafer is placed into the annealing equipment for annealing at a temperature of 925 °C for 50 min, and finally the doped amorphous silicon crystallizes to form

phosphorus-doped polysilicon (D12661, HORIS). (6) Then RCA cleaning, the specific process is as follows: firstly, the front side of the wafer is downward, through the chain hydrofluoric acid solution, to remove the PSG oxides on the front side, then the wafer is put into the tank KOH & additives solution, to remove the n⁺ poly-Si wraparound on the front side of the wafer. Finally, the wafer is placed in a tank hydrofluoric acid solution to remove oxides such as BSG on the front side and PSG on the rear side of the wafer. (7) An AlO_x layer was deposited on the front side of the wafer by tube-ALD equipment (Leadmicro). The precursor used was Trimethyl Aluminum (TMA) and the thickness of AlO_x was 5 nm. (8) Then a silicon nitride layer was grown on the front side of the wafer as well as on the back side by PECVD method (P12682, HORIS). The front side of SiN_x thickness is 75 nm, and the rear side of SiN_x thickness is 82 nm (9) Finally, silver-aluminum and silver pastes are printed on the front and back side of the wafer using screen printing (Maxwell) and then sintered in a sintering furnace (Despatch) to form metal contacts and H-passivation.

2.3. Characterizations

Scanning electron microscopy (SEM, FEI Quanta FEG 250) was used to investigate the cross-sectional morphology of the samples. X-ray diffraction (XRD, DB-ADVANCE) was utilized to ascertain the crystalline phase of polysilicon with varying doping levels. Electrochemical capacitance-voltage (ECV, WEP CVP21) measurements were used to characterize the active dopants. Spectroscopic ellipsometry (SE, HORIBA UVISEL PLUS) was employed to ascertain the refractive indices (n) and extinction coefficients (k) of polycrystalline silicon films at varying concentrations of P-doping. The external quantum efficiency was tested by a solar cell quantum efficiency tester (EQE, YLight Technology Co., Ltd, 1000ADX). X-ray photoelectron spectroscopy (XPS, Thermo Fisher ESCALAB Xi⁺) was utilized to examine the effects of varying doping levels on the chemical bonding between silicon and phosphorus in polycrystalline silicon films. The minority carrier lifetime of the passivated structure was tested by means of a quasi-steady-state photoconductor (Sinton Instruments WCT-120) under symmetric passivation conditions with an injection density of $1 \times 10^{15} \text{ cm}^{-3}$. The unilateral J_0 was determined using the high injection method proposed by Kane and Swanson [20]. The contact resistivity (ρ_c) was measured by the transfer length method [21] (TLM, Ai-shine). The electrical performance parameters of TOPCon solar cells were evaluated using a Maxwell tester under standard test conditions of AM 1.5G spectra at 25 °C.

3. Results and discussion

The SEM cross-section of the baseline (single poly-Si/SiO_x) in Fig. 3(a) shows that the thickness of the single-layer poly-Si is 120 nm, consistent with the thickness of the poly-Si layer in the TOPCon structure used industrially. The image for the experimental group (Fig. 3(b)) (double poly-Si/SiO_x) reveals that the bottom layer thickness is 65 nm

and the top layer is 55 nm. It is evident that there is a clear delamination between the two poly-Si layers, with SiO_x forming the middle layer. This suggests that the experimental design of the TOPCon double poly-Si/SiO_x structure meets expectations and lays a foundation for further analysis. Furthermore, ECV tests comparing the single poly-Si/SiO_x and double poly-Si/SiO_x structures were conducted, as shown in Fig. 3(c) and (d). The outcomes confirmed that the polysilicon thickness in the single poly-Si/SiO_x structure was approximately 115 nm, consistent with the SEM results in Fig. 3(a). The baseline sample exhibits a gradual decline in P concentration between etching depths of 80–110 nm, suggesting that phosphorus doping in the single poly-Si/SiO_x is not entirely uniform. However, the smooth trend of the P concentration curve in the S3 sample indicates more uniform doping in the poly-Si. This is due to the fact that the higher the doping of phosphorus atoms in the top poly-Si layer, the easier it is to diffuse through the silicon oxide layer into the bottom poly-Si layer at the same diffusion time. In addition, the great difference between the performance of the baseline sample and the experimental sample in Fig. 6 confirms that the double structure has better phosphorus diffusion homogeneity. In contrast, the significant decrease in the P concentration curve of the S1 sample is attributed to its relatively low doping concentration, which hinders effective P atom diffusion. Additionally, the p-concentration profile of the double poly-Si/SiO_x structure shows a pronounced change at approximately 65 nm, due to the top silicon oxide layer impeding P diffusion. To further investigate whether the uniformity of phosphorus concentration is altered after metallization annealing and sintering, we tested ECV analysis comparing samples from the baseline and experimental groups before and after co-firing (Fig. S1). Fig. S1 shows that the phosphorus doping concentration profiles of the baseline samples and the S1, S2, S3 samples before and after co-firing did not change significantly. This indicates that metallization annealing has no effect on the phosphorus doping concentration uniformity. After phosphorus doping annealing,

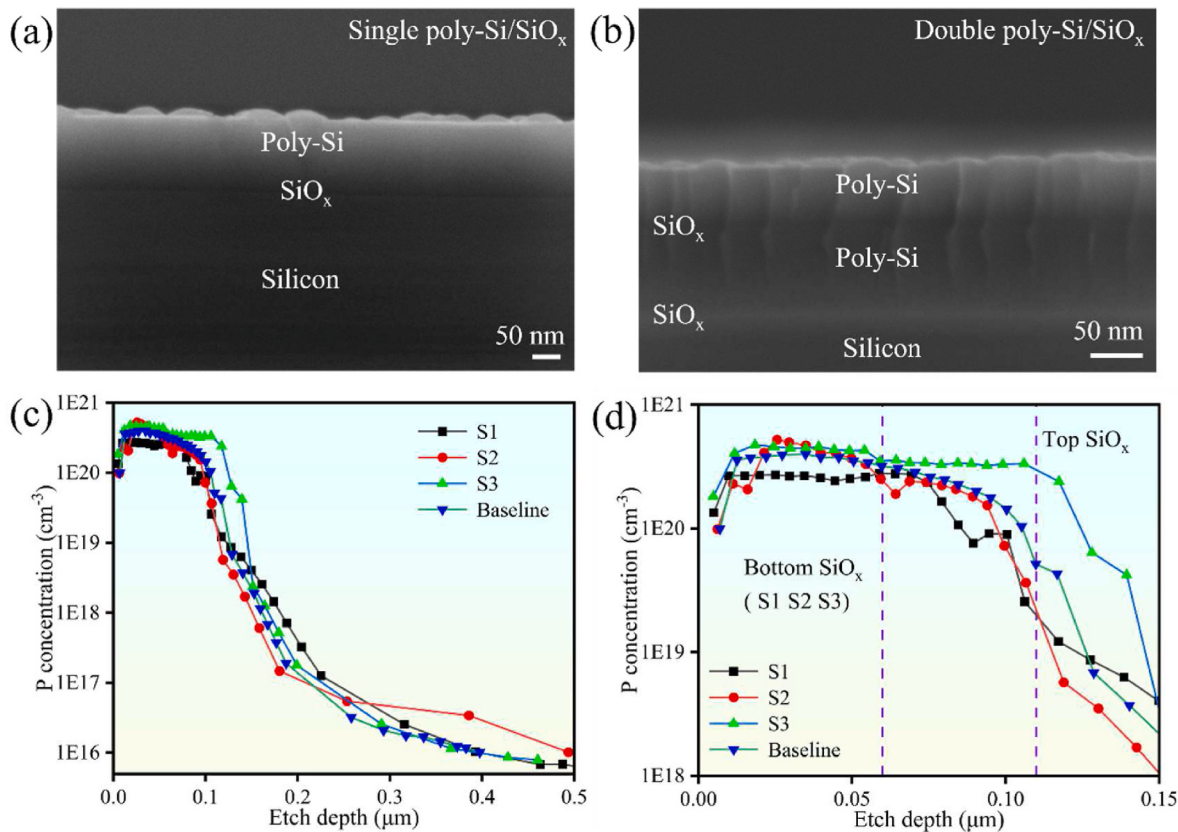


Fig. 3. (a) SEM cross-section of the baseline (single poly-Si/SiO_x); (b) SEM cross-section of the experimental group (double poly-Si/SiO_x); (c) Phosphorus doping concentration in sample poly-Si measured by ECV and (d) enlarge figure of the active P concentration in the poly-Si region of the sample measured by ECV.

the phosphorus doping concentration in polysilicon has been uniformly distributed. Comparison of the ECV curves reveals superior P-doping uniformity in the double poly-Si/SiO_x structure compared to the single poly-Si/SiO_x structure. This uniformity improvement benefits the passivation performance of TOPCon cells.

It is possible to investigate the accumulation and redistribution of polysilicon films with differing P-doping concentrations in the near surface region by analysing the changes to the chemical bonding states. In this study, X-ray photoelectron spectroscopy (XPS) analysis was employed to investigate and discuss the chemical bonding states of

polysilicon layers with varying P dopant concentrations, as detailed in Ref. [22]. Fig. 4(a) depicts a comprehensive XPS spectrum for polycrystalline silicon films from various samples. The spectra displayed therein correspond to peaks observed for Si 2s, Si 2p, O 1s, and C 1s. These findings align with those reported in the existing literature [23].

Fig. 4(b) depicts a magnified view of the 200–40 eV binding energy region, which allows for a comprehensive investigation of the peaks within this region. For quantitative analysis, the spectra in the P 2p region were curve-fitted using Gaussian-Lorentzian components, and the background subtraction work was carried out by Shirley shapes [24]. As

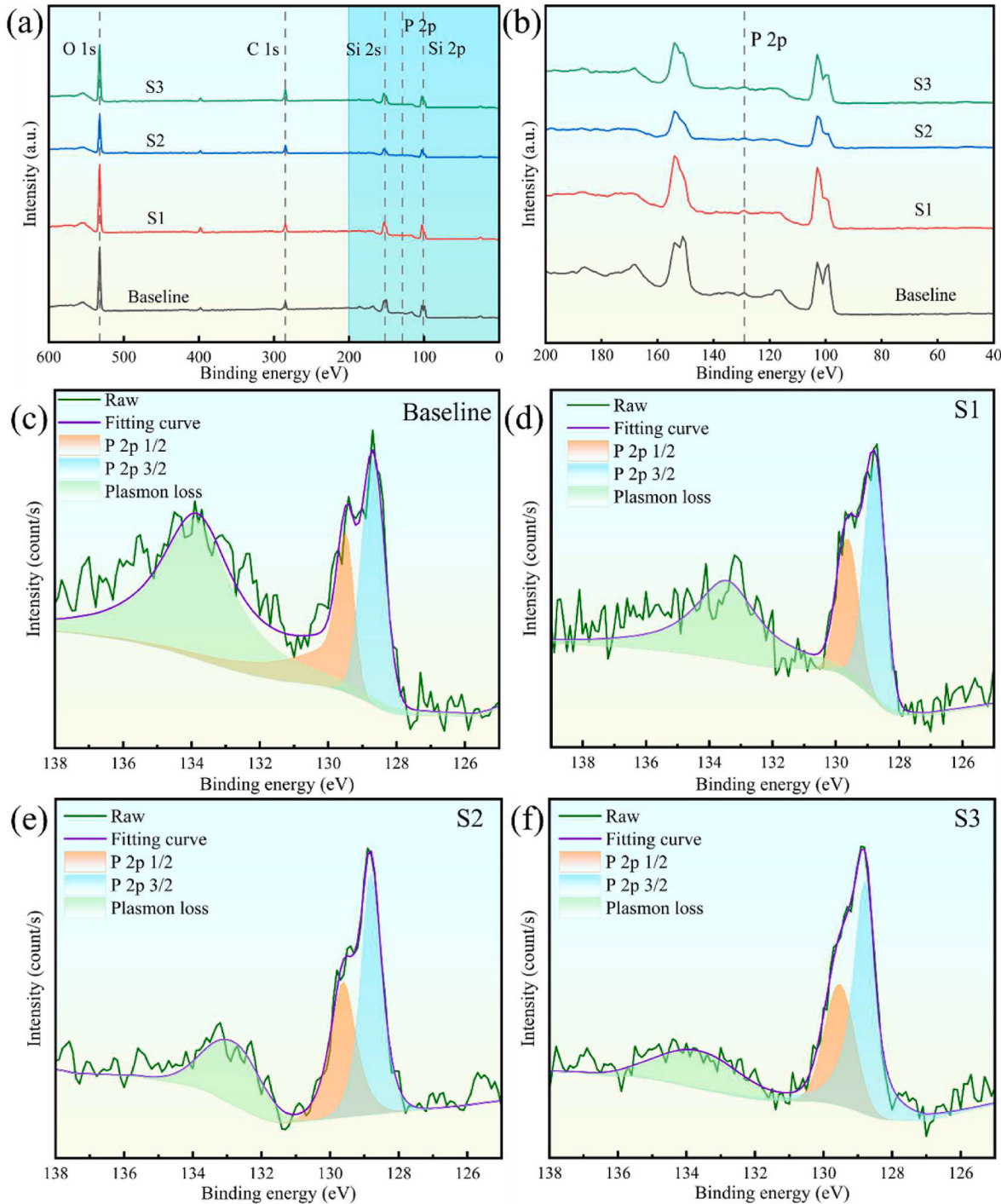


Fig. 4. (a) Full-range XPS spectra of polysilicon films from the baseline group and the experimental group; (b) Magnified images for the P 2p core-level region. (c)–(f) P 2p XPS spectra of (c) baseline, (d) S1, (e) S2 and (f) S3. The single-layer polysilicon/silicon oxide is denoted as baseline, and the lightly doped, moderately doped, and heavily doped samples of the underlying polysilicon in the double polysilicon/silicon oxide are denoted as S1, S2, and S3, respectively.

can be seen through Fig. 4(c–f), all the samples show broad peaks in the 135.0–133.0 eV region. According to previous reports, it is mainly the plasma loss peak of Si 2p, while the potential contribution of P–O bonds is small [25]. The binding energy bimodal peaks between 129.8 eV and 128.8 eV are mainly of P 2p_{1/2} and P 2p_{3/2} components, which suggests P doping by P bonding with Si [26]. The area ratio of the bimodal peaks is 1:2, and the spin-orbit splitting is between 0.90 and 0.95 eV, with a full width of less than 1.0 eV, which is in agreement with the previously reported value of 0.99 eV [27]. As expected, increasing P doping concentrations correspondingly raise the intensities of the P 2p_{1/2} and P 2p_{3/2} peaks. Experimental XPS observations clearly indicate that P atoms are integrated into the silicon lattice via PECVD in-situ doping and that Si–P bonding intensifies with increasing PH₃ flow rate.

Polycrystalline silicon materials are known to cause severe parasitic absorption losses due to their narrow band gap and high absorption coefficient. Therefore, the optical loss of polysilicon thin films has been investigated. The refractive index (n) and optical extinction coefficient (k) across the wavelength range of 250–1000 nm for various sample groups can be determined using spectroscopic ellipsometry, as shown in Fig. 5(a) and (b). Polycrystalline silicon thin-film materials are typically used on the backside of TOPCon solar cells, and it is observed that the optical properties of these materials are concentrated in the long-wavelength band range (600–1000 nm). When comparing n and k values for S1 samples at long wavelengths, it is evident that these diverge significantly from those of other samples. This indicates that there may be a high parasitic absorption in mildly P-doped polysilicon films. Upon the increase in the P-doping concentration to that of the S2

sample, the corresponding n and K values exhibited comparable behavior to that of the baseline in the long wavelength range. These findings indicate a gradual decline in parasitic absorption in polysilicon films as the phosphorus doping concentration reaches a threshold level. Furthermore, the parasitic absorption in the polysilicon film is found to be further reduced in the S3 group in comparison to the S2 group. Similarly, Fig. 5(c) illustrates the external quantum efficiency profiles of the samples compared to the baseline. The external quantum efficiency of the lightly doped (S1) sample significantly differs from that of the other samples in the long wavelength range. With increased phosphorus doping concentration, the external quantum efficiency in the long wavelength range for samples (S2 and S3) also improves, consistent with the data from Fig. 5(a) and (b). The aforementioned outcomes validate the hypothesis that parasitic absorption in polysilicon films begins to diminish when the concentration of dopants, specifically phosphorus, exceeds a specific threshold.

Fig. 5(d) illustrates the XRD patterns of the films. The figure displays three major silicon peaks corresponding to the (111), (220), and (311) orientations. It is well known that the reflection peaks of polysilicon films corresponding to the (111), (220), and (311) orientations occur at 2θ values of 28.4°, 47.3°, and 56.2°, respectively [28]. In contrast, the forbidden peak at 2θ = 33.1° for silicon (002), which has been attributed to multiple diffraction, was previously reported [29]. The XRD diffraction spectra show that the intensity of the (220) and (311) peaks increases with higher P doping concentrations, while the intensity of the (111) peak in the baseline sample remains almost unchanged compared to the S3 sample [30]. These findings suggest that P doping enhances the

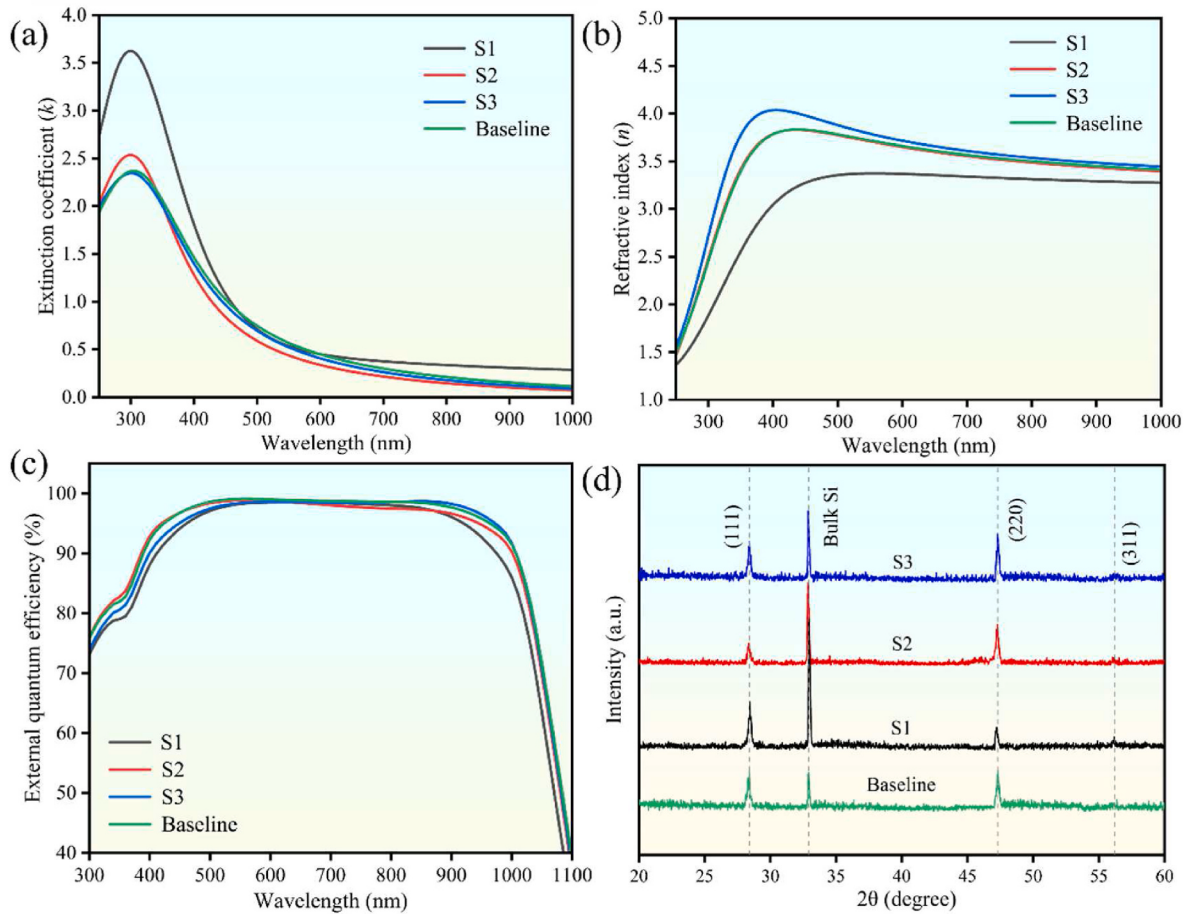


Fig. 5. a) and b) show the plots of extinction coefficient (k) and refractive index (n) of the sample as a function of wavelength measured by ellipsometry. (c) shows the external quantum efficiency plots for different samples and baseline. (d) XRD patterns of samples from the baseline groups and experimental groups, where the baseline is single layer polycrystalline silicon/silicon oxide structure; the experimental groups are lightly doped, moderately doped, and heavily doped double polycrystalline silicon/silicon oxide structure, corresponding to S1, S2, and S3, respectively.

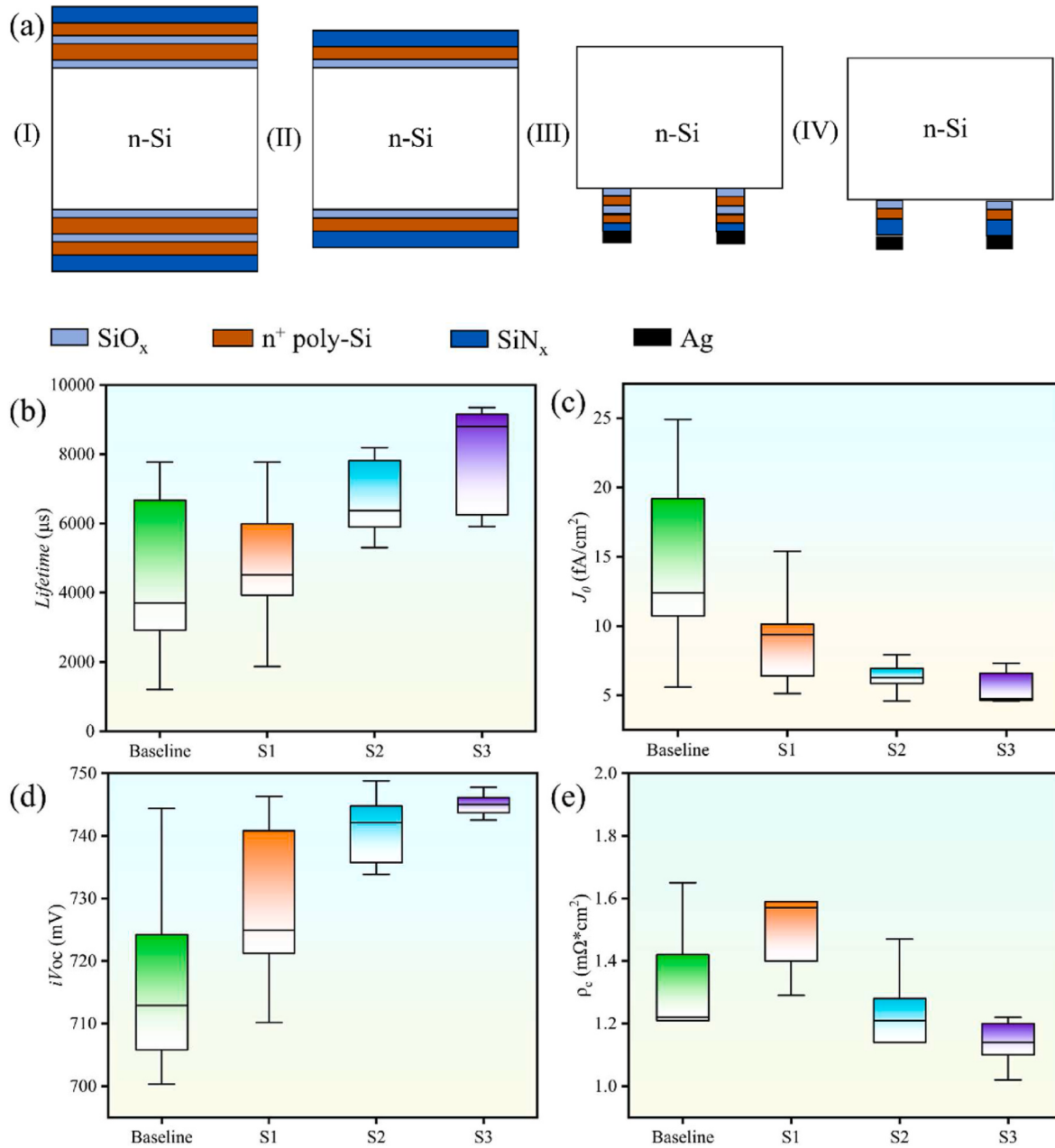


Fig. 6. (a) displays symmetrical structures for testing lifetime, J_0 , and $iVoc$ in (I)(II) and semi-finished structures for testing TLM contact resistance in (III)(IV). (b–e) are the test values of lifetime, J_0 , $iVoc$ and ρ_c , where baseline is single poly-Si/ SiO_x , S1, S2 and S3 are double poly-Si/ SiO_x structures, for using light doping, moderately doping and heavy doping, respectively.

crystallinity of amorphous silicon during annealing, contributing to the passivation effect in polysilicon films [31].

To further investigate the passivation performance of double poly-Si/ SiO_x structures at various P-doping levels, we studied and analyzed the passivation and contact resistance of TOPCon solar cells. Fig. 6(a) displays symmetrical structures for testing lifetime, J_0 , and $iVoc$ in (I)(II) and semi-finished structures for testing TLM contact resistance in (III)(IV). Fig. 6(b–e) illustrate the corresponding results for passivation and contact properties. As shown in Fig. 6(b), the lifetime increases from 4886 μs to 8030 μs as the doping concentration rises from S1 to S3. Also, it can be seen from the lifetime curves in Fig. S2 that the lifetime shows a gradual increase from baseline to S3. Similarly, J_0 decreases from 8.9 fA/cm^2 to 5.4 fA/cm^2 (Fig. 6(c)) and $iVoc$ increases from 728 mV to 744 mV (Fig. 6(d)). This improvement in passivation performance may stem from the enhanced field passivation capability of the polysilicon as the P

doping content increases. For the baseline single poly-Si/ SiO_x structure, the lifetime, J_0 , and $iVoc$ values are 4469 μs , 14.3 fA/cm^2 , and 717 mV, respectively. As illustrated in Fig. 6(b–d), the variation in passivation values for the baseline is considerably greater than that for the double poly-Si/ SiO_x structure. This suggests that the double poly-Si/ SiO_x significantly impacts the homogeneity of the P doping concentration in the underlying polysilicon [32]. This indicates that the second silicon oxide layer impedes the diffusion of P into the underlying polysilicon, leading to slower diffusion rates. Consequently, the doping of the underlying polysilicon becomes more uniform and controllable. As shown in Fig. S3, due to the high doping nature of polycrystalline silicon, this can lead to lateral conduction, which greatly affects contact resistivity measurements. For accurate measurements using the TLM method, the poly silicon between the fingers needs to be etched and it is ensured that the doped polycrystalline structure is located only underneath the finger

structure. The etching method can be done by using SiN_x as a mask layer, etching between the finger structures using laser and alkaline solution, and finally metallization. This will ensure that the current is transferred from one finger to the next through the silicon substrate rather than through the polysilicon. In Fig. 6(e), the contact properties of the passivation layer and the baseline were analyzed using TLM for different P doping concentrations. From Fig. 6(e), in the S1 sample, the corresponding contact resistivity reaches $1.59 \text{ m}\Omega \text{ cm}^2$, higher than that of the other samples. In contrast, the contact resistivity values for S2 and S3 are lower than those of the baseline, averaging $1.13 \text{ m}\Omega \text{ cm}^2$. In addition, the dark I-V curves (Fig. S4) of contact resistivity from S1 to S3 show an increasing slope, which indicates a decreasing contact resistivity. These observations reinforce the importance of the double poly-Si/ SiO_x design for P-doped polysilicon, effectively slowing down the diffusion of P into the underlying polysilicon layer, resulting in more uniform and controllable doping levels of the underlying polysilicon and enhanced passivation. This strategic addition can also facilitate the further fine-tuning of the doping profile, which in turn facilitates the development of high-efficiency solar cells.

To assess the device-level performance of $183 \times 183 \text{ cm}^2$ wafers, TOPCon solar cells utilizing a double structured passivation layer were fabricated, varying P doping (S1, S2, S3). The electrical performance parameters of these devices are detailed in Fig. 7. The observed changes in V_{oc} were consistent with previously measured changes in $iVoc$. Notably, the S3 group had the highest average V_{oc} value of 722.7 mV , which was 2.7 mV higher than the baseline average of 720.0 mV , indicating a significant increase in the level of passivation. Notably, the V_{oc} of baseline samples seems to be better than the mean $iVoc$. We suggest that this may be due to the insufficient passivation level of poly-Si itself

in the baseline sample set, which was co-firing and annealed after being prepared as a cell, so that hydrogen passivation in the silicon nitride film repaired the defects in the poly-Si passivation [33]. However, the passivation level of the poly-Si itself in the experimental group was excellent enough to make the hydrogen passivation effect in the silicon nitride film appear less pronounced after it was prepared into solar cells. As a result, there is a difference in the trend of V_{oc} and $iVoc$ performance between the samples of the baseline group and the samples of the experimental group. The short-circuit current density (J_{sc}) values for the S3 group were unchanged compared to the baseline, suggesting no additional light absorption losses due to the bilayer structure. The average fill factor (FF) increased from 83.00% to 83.39% , suggesting improved metal contact with the bilayer structure. In addition, Fig. S5 shows the J-V curves of the electrical performance of solar cell wafers with single poly-Si/ SiO_x and double poly-Si/ SiO_x structures. This improvement stems from the double poly-Si/ SiO_x structure's enhanced doping uniformity in the underlying polysilicon layer, improving contact quality. The most significant finding is the improvement in conversion efficiency (η), which increased by an average of 0.23% from 24.50% to 24.73% . This improvement is largely attributed to the increases in V_{oc} and FF. These results demonstrate that the double poly-Si/ SiO_x structure enhances both the passivation performance and contact quality of the cell.

In addition, we suggest that this structure is also applicable to the p^+ poly-Si contact because the double p^+ poly-Si/ SiO_x structure can also regulate the boron doping uniformity of the underlying poly and reduce the boron internal diffusion [5,34–36]. This structure will be very useful in the P-region of the rear junction devices on n-type substrates, and we believe that the conversion efficiency of the cell can be improved by

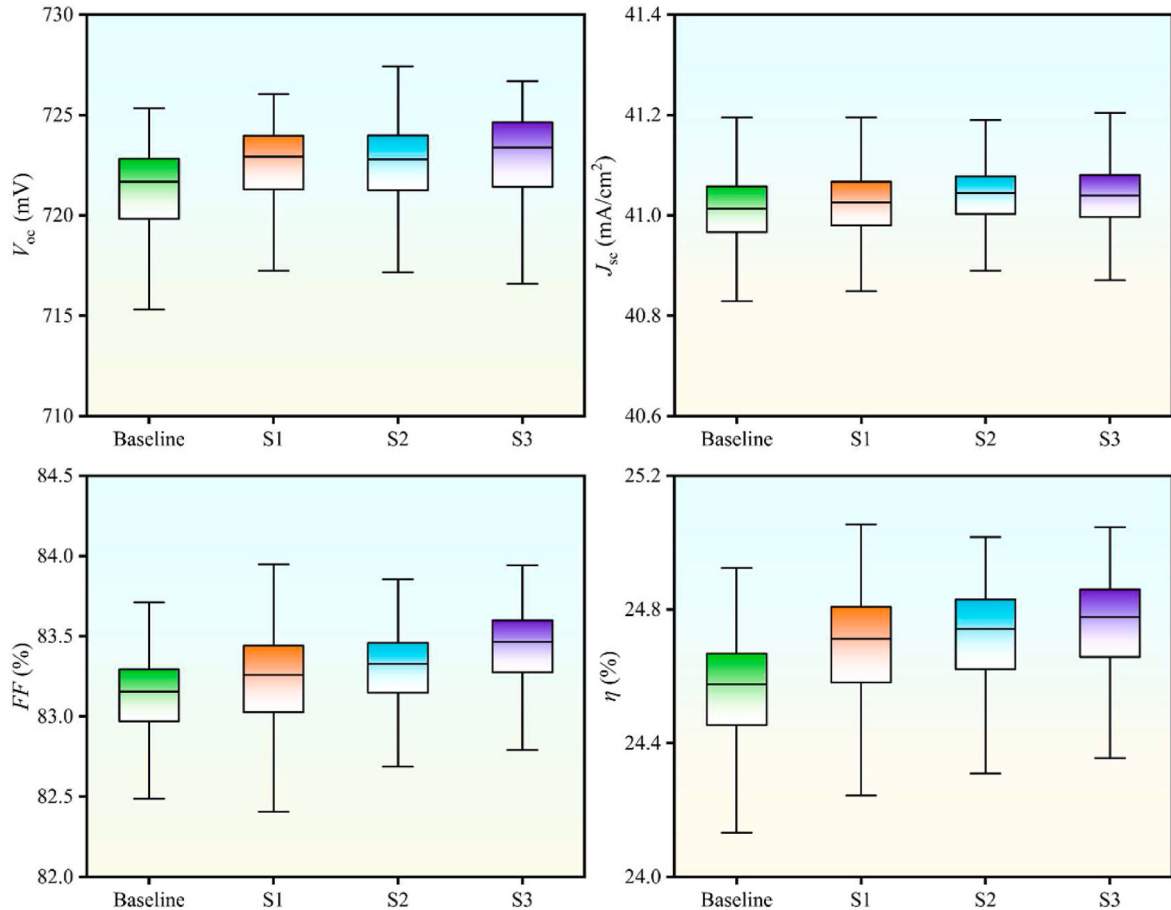


Fig. 7. Electrical performance test data using bilayer polysilicon/silicon oxide structured solar cells and baseline structured solar cells, samples from different experimental groups are denoted by S1, S2, and S3, respectively.

introducing a double n⁺ poly-Si/SiO_x structure in the N-region of the rear junction devices on p-type substrates.

4. Conclusions

In summary, this study demonstrates that the in-situ P-doped double poly-Si/SiO_x structure, fabricated via tube-PECVD, effectively improves polysilicon passivation and contact resistance, thereby enhancing the performance of TOPCon structures. This approach provides a simple, effective and mass-producible path to efficiency improvement in TOPCon solar cells. This work offers a detailed examination of the underlying mechanisms. SEM cross-sections show that the experimentally designed double poly-Si/SiO_x structure aligns with anticipated assumptions and lays the groundwork for further analysis. X-ray diffraction (XRD) results indicate that post-annealing P doping enhances the crystallinity of polysilicon. X-ray photoelectron spectroscopy (XPS) reveals that the incorporation of P atoms into polysilicon films increases with the PH₃ flow rate reaching a critical value. The analysis facilitated strategic adjustments to the P doping profile of the underlying polysilicon layer to optimize passivation contact. The optical properties were measured by ellipsometry, and the external quantum efficiency was determined by a quantum efficiency tester. The results show that the parasitic absorption of polysilicon films is reduced by increasing the P doping concentration of the polysilicon layer. This is also confirmed by passivation tests and resistivity tests, which indicate that the double polysilicon/silicon oxide structure has better electrical properties compared to the baseline structure. Finally, an industrial-scale TOPCon solar cell based on the double poly-Si/SiO_x structure achieved an average conversion efficiency of 24.73 %, 0.23 % higher than the baseline production TOPCon cell at 24.50 %. The results confirm that the proposed in situ P-doped double poly-Si/SiO_x structure via PECVD can enhance cell conversion efficiency and holds significant potential for industrial production. Furthermore, with higher deposition rates and reduced consumable usage, tube-PECVD offers a compelling alternative to conventional LPCVD for fabricating TOPCon solar cells.

CRediT authorship contribution statement

Wangchao Wan: Writing – review & editing, Writing – original draft, Software, Resources, Methodology, Investigation, Formal analysis, Data curation. **Jindou Shi:** Writing – review & editing. **Yixi Liang:** Writing – review & editing. **Chen Zhang:** Resources. **Zheyuan Da:** Resources. **Junnan Wang:** Resources. **Qing Yao:** Resources. **Youlong Xu:** Writing – review & editing. **Minqiang Wang:** Writing – review & editing, Supervision.

Declaration of competing interest

The authors declare that they have no known competing financial interests or personal relationships that could have appeared to influence the work reported in this paper.

Data availability

No data was used for the research described in the article.

Acknowledgements

This work received funding from the National Key R&D Program of China (2022YFE0122500 and 2019YFB1503200), the National Natural Science Foundation of China (NSFC, 52161145103 and 61774124), the 111 Program (No. B14040), and the Shaanxi Provincial Key Research and Development Program (No.2021GXHL-Z-084).

Appendix A. Supplementary data

Supplementary data to this article can be found online at <https://doi.org/10.1016/j.solmat.2024.113068>.

References

- [1] J. Sheng, Z.J. Ma, W.H. Cai, Z.Z. Ma, J.N. Ding, N.Y. Yuan, C. Zhang, Impact of phosphorus diffusion on n-type poly-Si based passivated contact silicon solar cells, Sol Energ Mat Sol C 203 (2019).
- [2] H. Park, H. Park, S.J. Park, S. Bae, H. Kim, J.W. Yang, J.Y. Hyun, C.H. Lee, S. H. Shin, Y. Kang, H.S. Lee, D. Kim, Passivation quality control in poly-Si/SiO_x/c-Si passivated contact solar cells with 734 mV implied open circuit voltage, Sol Energ Mat Sol C 189 (2019) 21–26.
- [3] J. Kim, H.-J. Kim, Y. Ko, Y. Kim, Ieee, development of machine vision system for detection of Wrap-around in n-TOPCon solar cells, in: IEEE 50th Photovoltaic Specialists Conference (PVSC), 2023, San Juan, PR.
- [4] Y. Chen, H. Chen, S. Zhang, L. Wang, C. Liu, D. Chen, J. Xu, P. Altermatt, Z. Feng, P. Verlinden, WP N-type I-TOPCon Modules in Mass Production with >25% Efficiency Solar Cells Based on Large-Area 210 Mm Wafers, 2023, 690.
- [5] R. Basnet, D. Yan, D. Kang, M.M. Shehata, P. Phang, T. Truong, J. Bullock, H. Shen, D. Macdonald, Current status and challenges for hole-selective poly-silicon based passivating contacts, Appl. Phys. Rev. 11 (2024).
- [6] W. Long, S. Yin, F.G. Peng, M. Yang, L. Fang, X.N. Ru, M.H. Qu, H.F. Lin, X.X. Xu, On the limiting efficiency for silicon heterojunction solar cells, Sol Energ Mat Sol C 231 (2021).
- [7] D. Ma, W. Liu, M. Xiao, Z. Yang, Z. Liu, M. Liao, Q. Han, H. Cheng, H. Xing, Z. Ding, B. Yan, Y. Wang, Y. Zeng, J. Ye, Highly improved passivation of PECVD p-type TOPCon by suppressing plasma-oxidation ion-bombardment-induced damages, Sol. Energy 242 (2022) 1–9.
- [8] Q. Wang, H. Peng, S. Gu, K. Guo, W. Wu, B. Li, L. Li, N. Yuan, J. Ding, High-efficiency n-TOPCon bifacial solar cells with selective poly-Si based passivating contacts, Sol Energ Mat Sol C 259 (2023).
- [9] Z. Kiaee, T. Fellmeth, B. Steinhauser, C. Reichel, M. Nazarzadeh, A.-C. Noelken, R. Keding, TOPCon silicon solar cells with selectively doped PECVD layers realized by inkjet-printing of phosphorus dopant sources, IEEE J. Photovoltaics 12 (2022) 31–37.
- [10] X. Zhang, L. Li, P. Shen, Z. Li, G. He, S. Zhang, B. Yu, J. Wang, D. Zhang, L. Liu, B. Zhang, Q. Yu, L. Cheng, Processing method of N-type TOPCon battery coating bad sheet, involves soaking first acid washing bad sheet into mixed acid solution of hydrofluoric acid and hydrochloric acid for acid washing, and washing with water after acid washing, in, Yingli Energy Dev Co Ltd; Yingli Energy Dev Baoding Co Ltd.
- [11] J. Zhou, B. Lv, H. Liang, Z. Wen, Simulation and optimization of polysilicon thin film deposition in a 3000 mm tubular LPCVD reactor, Sol. Energy 253 (2023) 462–471.
- [12] B. Liao, W. Wu, R.J. Yeo, X. Wu, S. Ma, Q. Wang, Y. Wan, X. Su, W. Shen, X. Li, W. Li, G. Xing, B. Hoex, Atomic scale controlled tunnel oxide enabled by a novel industrial tube-based PEALD technology with demonstrated commercial TOPCon cell efficiencies > 24, Progress in Photovoltaics 31 (2023) 220–229.
- [13] Z. Liu, N. Lin, Q. Zhang, B. Yang, L. Xie, Y. Chen, W. Li, M. Liao, H. Chen, W. Liu, Y. Wang, S. Huang, B. Yan, Y. Zeng, Y. Wan, J. Ye, 24.4% industrial tunnel oxide passivated contact solar cells with ozone-gas oxidation Nano SiO_x and tube PECVD prepared in-situ doped polysilicon, Sol Energ Mat Sol C 243 (2022).
- [14] P. Duy Phong, S. Lee, M.Q. Khokhar, S. Chowdhury, H. Park, Y. Kim, E.-C. Cho, J. Yi, Innovative passivating contact using quantum well at poly-Si/c-Si interface for crystalline silicon solar cells, Chem. Eng. J. 423 (2021).
- [15] D.P. Pham, S. Kim, D. Vinh-Ai, Y. Kim, J. Yi, Quantum-well passivating contact at polysilicon/crystalline silicon interface for crystalline silicon solar cells, Chem. Eng. J. 449 (2022).
- [16] S. Ma, B. Liao, D.X. Du, D. Ding, C. Gao, Z.P. Li, Q. Wang, X.Y. Wu, S. Zou, X. Su, R. J. Yeo, X. Li, W.M. Li, X.Y. Kong, W.Z. Shen, Bi-layer in-situ phosphorus doped poly-Si films by PECVD for blistering-free high-efficiency industrial TOPCon solar cells, Sol Energ Mat Sol C 269 (2024).
- [17] R. Glatthaar, F.-P. Schmidt, A. Hammud, T. Lunkenbein, T. Okker, F. Huster, S. Seren, B.C. Greven, G. Hahn, B. Terheiden, Silver metallization with controlled etch stop using SiO_x layers in passivating contacts for improved silicon solar cell performance, Sol. RRL 7 (2023).
- [18] R. Sharma, A. Alleva, A. Hajjiah, H.S. Radhakrishnan, J. Poortmans, Comparison of C-, N-, and O-incorporated non-blistering PECVD Si films for application in SiO_x-based passivating contacts for Si solar cells, ACS Appl. Energy Mater. 5 (2022) 9994–10001.
- [19] E. Lohmueller, P. Baliozian, L. Gutmann, L. Kniffki, V. Beladiya, J. Geng, L. Wang, R. Dunbar, A. Lepert, M. Hofmann, A. Richter, J.D. Huyeng, Thermal laser separation and high-throughput layer deposition for edge passivation for TOPCon shingle solar cells, Sol Energ Mat Sol C 258 (2023).
- [20] R.A. Sinton, A. Cuevas, Contactless determination of current-voltage characteristics and minority-carrier lifetimes in semiconductors from quasi-steady-state photoconductance data, Appl. Phys. Lett. 69 (1996) 2510–2512.
- [21] A. Fell, C. Reichel, T. Fellmeth, C. Luderer, F. Feldmann, M. Hermle, S.W. Glunz, Ieee, why and how to measure the non-metallized contact resistivity of a passivating contact, in: 47th IEEE Photovoltaic Specialists Conference (PVSC), Electr Network, 2020, pp. 884–889.

- [22] I.S. Tilinin, A. Jablonski, W.S.M. Werner, Quantitative surface analysis by Auger and x-ray photoelectron spectroscopy, *Prog. Surf. Sci.* 52 (1996) 193–335.
- [23] M. Ramstedt, L. Leone, A. Shchukarev, *Bacterial Surfaces in Geochemistry - How Can X-Ray Photoelectron Spectroscopy Help?*, 2019.
- [24] G.G. Wepfer, T.C. Collins, R.N. Euwema, Calculated SPIN-orbit splittings of some group IV, III-V, and II-VI semiconductors, *Bull. Am. Phys. Soc.* 15 (1970) 1379. &
- [25] H.Y. Ryu, M. Lee, H. Park, D.H. Ko, Chemical bonding states and dopant redistribution of heavily phosphorus-doped epitaxial silicon films: effects of millisecond laser annealing and doping concentration, *Appl. Surf. Sci.* 504 (2020).
- [26] M. Lee, S. Kim, D.-H. Ko, Chemical state analysis of heavily phosphorus-doped epitaxial silicon films grown on Si (100) by X-ray photoelectron spectroscopy, *Appl. Surf. Sci.* 443 (2018) 131–137.
- [27] C.J. Powell, Elemental binding-energies for X-ray photoelectron-spectroscopy, *Appl. Surf. Sci.* 89 (1995) 141–149.
- [28] K. Chen, A. Bothwell, H. Guthrey, M.B. Hartenstein, J.-I. Polzin, F. Feldmann, W. Nemeth, S. Theingi, M. Page, D.L. Young, P. Stradins, S. Agarwal, Measurement of poly-Si film thickness on textured surfaces by X-ray diffraction in poly-Si/SiO_x passivating contacts for monocrystalline Si solar cells, *Sol Energ Mat Sol C* 236 (2022).
- [29] A.S. Kale, W. Nemeth, H. Guthrey, S.U. Nanayakkara, V. LaSalvia, S. Theingi, D. Findley, M. Page, M. Al-Jassim, D.L. Young, P. Stradins, S. Agarwal, Effect of crystallographic orientation and nanoscale surface morphology on poly-Si/SiO_x contacts for silicon solar cells, *Acs Applied Materials & Interfaces* 11 (2019) 42021–42031.
- [30] B. Birouk, D. Madi, Thermal oxidation effect on structural and optical properties of heavily doped phosphorus polycrystalline silicon films, *Appl. Phys. Mater. Sci. Process* 104 (2011) 739–748.
- [31] P. Zaumseil, High-resolution characterization of the forbidden Si 200 and Si 222 reflections, *J. Appl. Crystallogr.* 48 (2015) 528–532.
- [32] X.H. Geng, J.M. Xue, H.C. Ge, H.B. Li, Z.P. Wang, Z.Q. Wang, H.Z. Ren, Modeling of a-Si/poly-Si and a-Si/poly-Si/poly-Si stacked solar cells, *Sol Energ Mat Sol C* 75 (2003) 489–495.
- [33] D. Kang, H.C. Sio, J. Stuckelberger, D. Yan, S.P. Phang, R. Liu, T.N. Truong, T. Le, H.T. Nguyen, X. Zhang, D. Macdonald, Comparison of firing stability between p- and n-type polysilicon passivating contacts, *Progress in Photovoltaics* 30 (2022) 970–980.
- [34] H. Park, J. Kim, D. Choi, S.-W. Lee, D. Kang, H.-S. Lee, D. Kim, M. Kim, Y. Kang, Boron-doped polysilicon using spin-on doping for high-efficiency both-side passivating contact silicon solar cells, *Progress in Photovoltaics* 31 (2023) 461–473.
- [35] J. Stuckelberger, D. Yan, S.P. Phang, C. Samundsett, J. Wang, L. Antognini, F.-J. Haug, Z. Wang, J. Yang, P. Zheng, X. Zhang, D. Macdonald, Pre-annealing for improved LPCVD deposited boron-doped poly-Si hole-selective contacts, *Sol Energ Mat Sol C* 251 (2023).
- [36] A.R. Sitaram, S.P. Murarka, T.T. Sheng, Grain-Growth in boron doped LPCVD polysilicon films, *J. Mater. Res.* 5 (1990) 360–364.